Atmos. Meas. Tech., 12, 5639–5653, 2019
https://doi.org/10.5194/amt-12-5639-2019

Atmospheric Measurement Techniques
Open Access
EGU

Development of a balloon-borne instrument for CO_2 vertical profile observations in the troposphere

Mai Ouchi[1], Yutaka Matsumi[1], Tomoki Nakayama[2], Kensaku Shimizu[3], Takehiko Sawada[3], Toshinobu Machida[4], Hidekazu Matsueda[5], Yousuke Sawa[5], Isamu Morino[4], Osamu Uchino[4], Tomoaki Tanaka[6,a], and Ryoichi Imasu[7]

[1]Institute for Space-Earth Environmental Research and Graduate School of Science, Nagoya University, Furo-cho, Chikusa-ku, Nagoya, Aichi 464-8601, Japan
[2]Graduate School of Fisheries and Environmental Sciences, Nagasaki University, 1-14, Bunkyo-machi, Nagasaki, Nagasaki 852-8521, Japan
[3]Meisei Electric Co., Ltd., 2223 Naganumamachi, Isesaki, Gunma 372-8585, Japan
[4]National Institute for Environmental Studies, 16-2 Onogawa, Tsukuba, Ibaraki 305-8506, Japan
[5]Meteorological Research Institute, Japan Meteorological Agency, 1-1 Nagamine, Tsukuba, Ibaraki 305-0052, Japan
[6]Japan Aerospace Exploration Agency Earth Observation Research Center, 2-1-1, Sengen, Tsukuba, Ibaraki 305-8505, Japan
[7]Atmosphere and Ocean Research Institute, The University of Tokyo, 5-1-5, Kashiwanoha, Kashiwa, Chiba 277-8568, Japan
[a]now at: NASA Ames Research Center, Moffett Field Mountain View, CA 94035, USA

Correspondence: Yutaka Matsumi (matsumi@nagoya-u.jp)

Received: 23 October 2018 – Discussion started: 3 January 2019
Revised: 16 September 2019 – Accepted: 17 September 2019 – Published: 24 October 2019

Abstract. A novel, practical observation system for measuring tropospheric carbon dioxide (CO_2) concentrations using a non-dispersive infrared analyzer carried by a small helium-filled balloon (CO_2 sonde) has been developed for the first time. Vertical profiles of atmospheric CO_2 can be measured with a 240–400 m altitude resolution through regular onboard calibrations using two different CO_2 standard gases. The standard deviations (1σ) of the measured mole fractions in the laboratory experiments using a vacuum chamber at a temperature of 298 K were approximately 0.6 ppm at 1010 hPa and 1.2 ppm at 250 hPa. Two CO_2 vertical profile data obtained using the CO_2 sondes, which were launched on 31 January and 3 February 2011 at Moriya, were compared with the chartered aircraft data on the same days and the commercial aircraft data obtained by the Comprehensive Observation Network for TRace gases by Airliner (CONTRAIL) program on the same day (31 January) and 1 d before (2 February). The difference between the CO_2 sonde data and these four sets of in situ aircraft data (over the range of each balloon altitude ±100 m) up to the altitude of 7 km was 0.6 ± 1.2 ppm (average $\pm 1\sigma$). In field experiments, the CO_2 sonde detected an increase in CO_2 concentration in an urban area and a decrease in a forested area near the surface. The CO_2 sonde was shown to be a useful instrument for observing and monitoring the vertical profiles of CO_2 concentration in the troposphere.

1 Introduction

Atmospheric carbon dioxide (CO_2) is one of the most important anthropogenic greenhouse gases for global warming. Certain human activities, such as fossil fuel combustion, cement production, and deforestation, are the major cause of atmospheric CO_2, making the global average concentration of atmospheric CO_2 increase from 280 ppm before the Industrial Revolution to 400.0 ppm in 2015 (World Meteorological Organization, WMO, 2016). Over the last 10 years, the average rate of atmospheric CO_2 increase is measured at 2.21 ppm yr^{-1} (WMO, 2016). Atmospheric CO_2 is measured by ground-based stations and ships using the flask sampling and continuous instrument methods such as non-dispersive infrared absorption (NDIR) (Tanaka et al., 1983; Hodgkinson et al., 2013) and cavity ring-down spectroscopy (CRDS) (Winderlich et al., 2010). A network of ground-based Fourier transform spectrometers (FTS) that record the

direct solar spectra in the near-infrared spectral region (Total Carbon Column Observing Network, TCCON) is used to observe the column-averaged mole fraction of CO_2 in dry air (total column XCO_2) (Wunch et al., 2011). These observations have provided extensive information regarding the distribution and temporal variation of CO_2 in the atmosphere (Pales and Keeling, 1965; Conway et al., 1988; Komhyr et al., 1989; Tans et al., 1989; Conway et al., 1994). Moreover, atmospheric CO_2 measurement data are useful for estimating CO_2 fluxes at the surface through inverse modeling (Gurney et al., 2004; Baker et al., 2006). Due to the limited number of observation sites and the limitations of their altitudinal range, a large degree of uncertainty in the current estimates of the regional CO_2 sources and sinks is noted (Gurney et al., 2002). More atmospheric CO_2 measurements are needed to reduce the uncertainties in CO_2 flux estimation using an inverse modeling.

To address the issues with insufficient CO_2 observational data, satellite remote sensing techniques have been used to investigate the CO_2 distribution on a global scale (Chédin et al., 2002; Crevoisier et al., 2004; Dils et al., 2006). The Greenhouse Gases Observing SATellite (GOSAT), which measures the short wavelength infrared (SWIR) spectra of sunlight reflected by the earth's surface with a Fourier transform spectrometer and obtains the total column XCO_2, has been in operation since early 2009 (Yokota et al., 2009; Yoshida et al., 2011; Morino et al., 2011). Since 2014, the Orbiting Carbon Observatory-2 (OCO-2) satellite has also measured the IR spectra of the surface-reflected sunlight with a diffraction grating spectrometer and obtains total column XCO_2 (Eldering et al., 2017). However, these satellite observations provide only nadir total column XCO_2 and do not measure the vertical distributions of CO_2 concentrations, as the observed spectra of the surface-reflected sunlight do not provide enough information to determine the vertical distributions. Furthermore, the satellites overpass a specific earth-based target once several days only at about noon in the solar time because of their sun-synchronous orbits.

The altitude distributions of CO_2 concentrations have been measured using other techniques. For instance, tall towers measure vertical profiles of CO_2 near the ground (Bakwin et al., 1992; Inoue and Matsueda, 2001; Andrews et al., 2014). CO_2 vertical profiles up to 10 km near the airports have been observed by the equipment installed by the commercial airlines, such as the Comprehensive Observation Network for TRace gases by Airliner (CONTRAIL program) (Machida et al., 2008; Matsueda et al., 2008). Measurements by equipment installed on chartered aircrafts have also been undertaken, which include the High-performance Instrumented Airborne Platform for Environmental Research (HIAPER), the Pole-to-Pole Observations (HIPPO) program up to 14 km at altitudes spanning the Pacific from 85° N to 67° S (Wofsy et al., 2011), the NIES/JAXA (National Institute of Environmental Studies and Japan Aerospace eXploration Agency) program at an altitude from 2 to 7 km (Tanaka et al., 2012), and the NOAA/ESRL Global Greenhouse Gas Reference Network Aircraft Program (Sweeney et al., 2015). Although these aircraft measurements provided the vertical profiles of CO_2 concentrations, vertical profile measurements using the commercial airlines are limited around the large airports, and the frequency of the measurements using chartered airplanes is often limited by their relatively high cost. The continuation and expansion of airborne measurement programs for CO_2 and related tracers are expected to enhance the estimation of the global carbon cycling greatly (Stephens et al., 2007).

Atmospheric CO_2 observations using balloons, to select specific locations unless prohibited or restricted by aircraft flight paths, are useful for solving the issues associated with the sparseness of CO_2 vertical data. Balloon-borne observations of stratospheric CO_2 were previously conducted by other studies. For instance, stratospheric air sampling was conducted using cryogenic sampler onboard balloons once a year from 1985 to 1995 over the northern part of Japan (Nakazawa et al., 1995). Balloon-borne near-infrared tunable diode laser spectrometers have been developed to provide in situ data for CO_2 in the stratospheric atmosphere (Durry et al., 2004; Joly et al., 2007; Ghysels et al., 2012). Furthermore, two in situ CO_2 analyzers adopting the NDIR technique, using a modified commercial detector for stratospheric measurements, have been developed for deployment on the NASA ER-2 aircraft and on a balloon (Daube et al., 2002). These balloon-borne instruments described above were specially designed to measure CO_2 concentrations in the stratosphere.

Observation of the CO_2 vertical distribution in the troposphere is essential because the uncertainties in the estimated fluxes, using the inverse method, can be attributed to the inaccurate representations of the atmospheric processes in transport models. Misrepresentation of vertical mixing by the transport models, particularly inside of the boundary layer, which is the layer closest to the ground where CO_2 is taken up and released, is one of the dominant causes of the uncertainty in CO_2 flux estimation (Stephens et al., 2007; Ahmadov et al., 2009). Recently, the observation of tropospheric CO_2 was conducted, using a lightweight unmanned aerial vehicle, such as a kite plane, with a commercial NDIR instrument. CO_2 profiles were observed in and above the planetary boundary layer up to 2 km to investigate the temporal and spatial variations of CO_2 (Watai et al., 2006). A passive air sampling system for atmospheric CO_2 measurements, using a 150 m long stainless-steel tube called an AirCore, was developed (Karion et al., 2010). The AirCore mounted on an airplane or a balloon ascends with evacuating inside of the tube to a high altitude of 30 km at flight maximum, then collecting ambient air by pressure changes along a decrease in altitude. The sampled air in the tube is analyzed with a precision of 0.07 ppm for CO_2 indicated as 1 standard deviation in the laboratory, and the vertical profile of CO_2 is obtained.

In the present study, we have developed a practical CO_2 sonde system that can measure in situ CO_2 vertical profiles in the atmosphere from the ground to altitudes up to about 10 km with a 240–400 m altitude resolution by using a small-sized balloon. Although the sonde system is thrown away after every flight due to the difficulties associated with recovery, the sonde systems are easily prepared with a relatively low cost. We have tested the sonde flight experiments more than 20 times in Japan. The CO_2 sonde developed has the following advantages, compared with other measurement techniques described above: (1) its cost of operation is low and flight permission is easy to obtain from the authorities as compared with the aircraft observations; (2) the CO_2 sonde can be easily carried to the launch sites since the instrument is light; (3) a limited amount of power is required for the operation; (4) it can generally be launched at any time; and (5) the meteorological data are obtained simultaneously with CO_2 profile data. In this study, the design of our novel CO_2 sonde and the results of the comparison experiments with aircraft measurements are described. The target accuracy and precision in the measurements with the CO_2 sonde are below about 1 ppm CO_2 mole fraction in the atmosphere of 400 ppm CO_2, preferable for carbon cycle studies (e.g., Maksyutov et al., 2008). The developed CO_2 sonde system attained virtually all the targets from the ground to an altitude of about 10 km.

Inai et al. (2018) measured vertical profiles of the CO_2 mole fraction in the equatorial eastern and western Pacific in February 2012 and February–March 2015, respectively, by using our novel CO_2 sondes which are described in this report. They found that the 1–10 km vertically averaged CO_2 mole fractions lie between the background surface values in the Northern Hemisphere (NH) and those in the Southern Hemisphere (SH) monitored at ground-based sites during these periods. Their study showed that the combination of CO_2 sonde measurements and trajectory analysis, taking account of convective mixing, was a useful tool in investigating CO_2 transport processes.

2 Materials and methods

2.1 Design of the CO_2 sonde

Many severe restrictions are noted for the operation of balloon-borne CO_2 sondes. First, the weight of the CO_2 sonde package should be less than about 2 kg, based on the legal restriction by the US FAA (Federal Aviation Administration) and by the Japanese aviation laws for the payload weight of 2.721 kg for unmanned free balloons. Balloon systems heavier than the above-regulation weight are not useful for the frequent flights because the flight permission from the authorities is much more difficult to obtain and the additional safety requirements are more expensive. The balloon system is thrown away in the ocean after each flight due to a long-distance transportation (100 km or more to the east) by strong westerly winds in the upper atmosphere of a mid-latitude area. This is done to avoid the accidents associated with falling onto urban areas, resulting in high recovery costs. Therefore, the cost of the CO_2 sonde system should be low for frequent observations. The non-recovery system implies that every instrument should perform consistently.

In this study the NDIR technique was adopted for a detection of CO_2 concentrations. The NDIR CO_2 measurement techniques have been widely used in many places such as WMO/GAW (Global Atmosphere Watch) stations. Our target instrumental accuracy and precision of approximately 1 ppm are less stringent than those of the ground-based instruments (± 0.1 ppm) used at the WMO/GAW stations (WMO, 2016). However, the surrounding conditions for the instrument are substantially severe during the flight experiments, as the pressure changes from 1000 to 250 hPa and the surrounding temperature changes from 300 to 220 K during flights from the surface to an altitude of 10 km in about 60 min.

In the NDIR technique for CO_2 measurements, the IR emission from a broadband wavelength source is passed through an optical cell and two filters, and then the light intensities are detected by two IR detectors. The one optical filter covers the whole absorption band of CO_2 around 4.3 µm, while the other covers a neighboring non-absorbed region around 4.0 µm provided that the chosen active and reference channel filters do not significantly overlap with the absorption bands of other gas species present in the application (Hodgkinson et al., 2013).

The Beer–Lambert law is expressed by Eq. (1), defining the light intensity in the absence of CO_2 in the cell as I_0 and the light intensity in the presence of CO_2 in the cell as I:

$$\frac{I}{I_0} = \exp(-\varepsilon C L), \tag{1}$$

where C is the CO_2 concentration in molec. cm^{-3}, L is the optical path length in centimeters, and ε is the absorption cross section in cm^2 $molecule^{-1}$. Using the relationship of $C = X P\ (k_B T)^{-1}$, where X is the CO_2 mole fraction and P is the pressure of dehumidified ambient air, and the approximation of $\exp(-\varepsilon C L) = 1 - \varepsilon C L$ under the condition of $\varepsilon C L \ll 1$, Eq. (1) is rewritten as

$$\frac{(I_0 - I)}{P} = X \frac{I_0 \varepsilon L}{k_B T_C}, \tag{2}$$

where T_c is the sample air temperature in the sensor cell and k_B is the Boltzmann constant. Equations (1) and (2) hold for monochromatic light only and Eq. (2) only holds for small absorptions. Although the NDIR analyzer exhibits nonlinear absorption due to the saturation of strong absorption lines, it is known to have a good linearity within a certain concentration range (Galais et al., 1985), and Eq. (2) may be used correspondingly. In our analyses of the balloon data,

Eq. (2) was used only for the interpolation between the low and high mole fractions of the in-flight calibration gases to obtain the ambient CO_2 mole fractions. With a 120 mm long absorption cell, the absorption intensity is approximately 3 % at 400 ppm CO_2 with our CO_2 NDIR system, i.e., $\varepsilon C L \approx 0.03$, and the approximations of $\exp(-\varepsilon C L) = 1 - \varepsilon C L$ are well fitted. The values of $[I(4.0) - I(4.3)]$ were used instead of $(I_0 - I)$ to obtain the CO_2 mole fraction values in the NDIR measurements, where $I(4.0)$ and $I(4.3)$ were the signal intensities at the 4.0 µm wavelength for background measurements and the 4.3 µm wavelength for CO_2 absorption measurements, respectively. Thus, the value of $[I(4.0) - I(4.3)]/P$ is proportional to the CO_2 mole fraction X in the optical cell. The proportionality constant is usually determined by the measurements of the standard gases. In the NDIR measurements at the ground WMO/GAW stations, carbon dioxide mole fractions are referenced to a high working standard and a low working standard and are determined by the interpolations of the signals with the two standards, and the calibrations with the two standard gases are carried out every 12 h (Fang et al., 2014).

2.2 System configuration of the CO_2 sonde system

A schematic diagram and photograph of the CO_2 measurement instrument are shown in Fig. 1. The CO_2 sonde has three inlets installed for ambient air and two calibration gases with mesh filters (EMD Millipore, Millex-HA, 0.45 µm pore size) to remove the atmospheric particles. Three solenoid valves (Koganei, G010LE1-21) were used to switch the gas flow to the CO_2 sensor. A constant-volume piston pump with a flow rate of 300 $cm^3\,min^{-1}$ (Meisei Electric co., Ltd.), which was originally used for ozonesonde instruments, directed the gas flows from the inlets through the solenoid valves into a dehumidifier, a flow meter, and a CO_2 sensor. The absolute STP (standard temperature and pressure) flow rate decreased with a decrease in pressure. Since the exit port of the CO_2 sensor was opened to the ambient air, the pressures of dehumidified outside air and calibration gases in the absorption cell were equal to the ambient pressure during the flight. Next to the pump, the gases were introduced into a glass tube filled with the magnesium perchlorate grains (dehumidifier) installed upstream of the CO_2 sensor to remove the water vapor. Fabric filters were installed on both ends of the dehumidifier, and a mesh filter was installed downstream of the dehumidifier to prevent the CO_2 sensor from the incursion of magnesium perchlorate grains to the optical cell.

The infrared absorption cell consisted of a gold-coated glass tube, a light source, and a photodetector. The light source (Helioworks, EP3963) consisted of a tungsten filament with a spectral peak intensity wavelength of approximately 4 µm. The light from the source passed through a gold-coated glass tube (length 120 mm and inside diameter 9.0 mm). The commercial CO_2 NDIR photodetector (PerkinElmer TPS2734) had two thermopile elements, one of which was equipped with a band-pass filter at a wavelength of 4.3 µm for the measurement of the CO_2 absorption signal, whereas the other was equipped with a band-pass filter at a wavelength of 4.0 µm for the measurement of the background signal. The signals from the sensors were amplified by an operational amplifier and converted to 16 bit digital values by an A/D convertor. The signal intensities of the detectors at 4.0 and 4.3 µm without CO_2 gas were set to the equal levels by adjusting the amplification factors in the laboratory. The electric power for the CO_2 sensor, pump, and valves was supplied through a control board using three 9 V lithium batteries, lasting for more than 3 h during the flight. The control board connected to the components regulated the measurement procedures, such as switching the solenoid valves and processing the signal. As shown in Fig. 1, the measurement system has an expanded polystyrene box molded specially to settle the optical absorption cell, electronic board, pump, battery, and other components.

2.3 Calibration gas package

Under the wide ranges of temperature and pressure conditions, the CO_2 sensor signal was unstable, and the calibration of the CO_2 sensor only on the ground before launch was insufficient to obtain the precise values of the CO_2 concentrations. To solve this problem, an in-flight calibration system was incorporated into the CO_2 sonde. A calibration gas package was attached to the CO_2 sonde for the in-flight calibration, as shown in Fig. 2. The calibration gas package consisted of two aluminum bags coated with polytetrafluoroethylene (PTFE) (maximum volume: 20 L), containing reference gases with low ($\sim$ 370 ppm) and high ($\sim$ 400 ppm) CO_2 concentrations. In each bag, $\sim$ 8 L (STP) of the reference gas was introduced from standard CO_2 gas cylinders just before launch. Since the gas bags were soft, their inner pressures were equal to the ambient air pressures during the balloon flight. The gas volumes in the bags increased with the altitude during the ascent of the balloon due to a decrease in the ambient pressure, while the reference gases were consumed during the calibration procedures. The optimum amounts of gas in the bags were determined by both the ascending speed of the balloon and the consumption rate to avoid the bursting of the bags and exhaustion of the gases. The CO_2 concentrations of the reference gases in the bags were checked by the NDIR instrument (LICOR, LI-840) before launching. Thereafter, approximately 6 L of the reference gas was left in each bag for a subsequent in-flight calibration. The change in the CO_2 mole fraction in the bags was less than 1 ppm over a 3 d period, which was negligible over the observation time during the balloon flight. All measurements were reported as dry-air mole fractions relative to the internally consistent standard scales maintained at Tohoku University (Tanaka et al., 1987; Nakazawa et al., 1992).

Since the gas exit port of the optical absorption cell was opened to the ambient air, the cell pressure was equalized

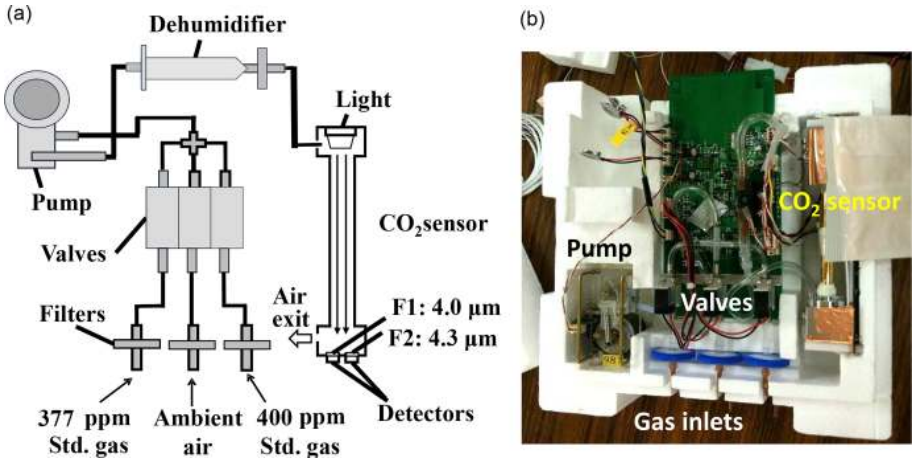

Figure 1. (a) Schematic diagram of the CO_2 measurement package, where F1 and F2 represent the band-pass filters at wavelengths of 4.0 and 4.3 µm, respectively. The outlet port of the CO_2 sensor is opened to ambient air. Details of the system are described in the text. **(b)** Photograph of the inside of the CO_2 sonde package. The components were placed in a specially modeled expanded polystyrene box.

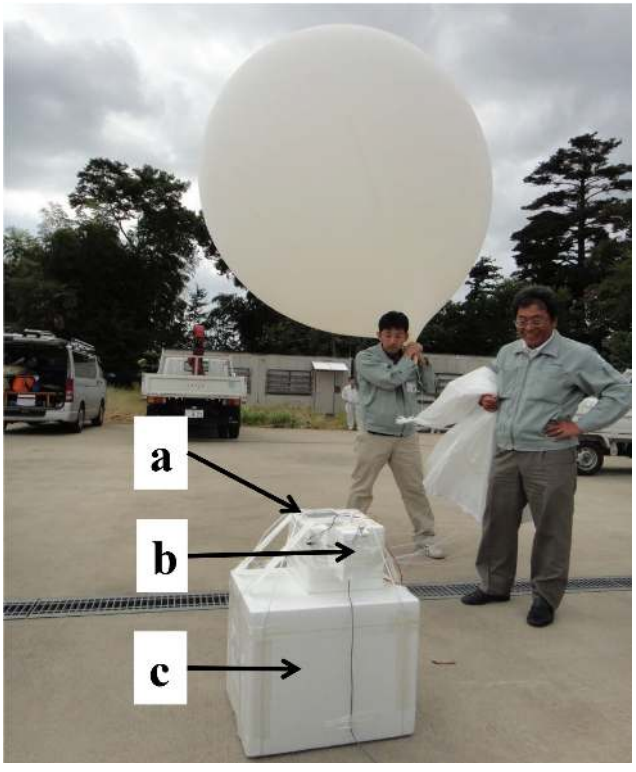

Figure 2. Photograph of the CO_2 sonde developed in this study before launching. **(a)** The CO_2 measurement package as shown in Fig. 1, **(b)** GPS sonde, and **(c)** calibration gas package.

with the ambient pressure for measuring both the ambient air and two standard gases. During the balloon-borne flights, the temperatures inside the CO_2 sonde package were measured with thermistors. The temperature inside the CO_2 sonde package gradually decreased by approximately 5 K, from 298 K on the ground to 293 K at an altitude of 10 km during the flights. Probably due to the polystyrene box and the heat produced by the NDIR lamp, pump, and solenoid valves, the temperature inside the sonde package remained virtually constant in spite of low ambient temperatures at high altitudes ($\sim$ 220 K). Within one measurement cycle time (160 s) with the standard gases, the temperature change was less than 0.4 K in the sonde package. The temperatures of the sample gas in the tube just before the inlet of the CO_2 NDIR cell were also measured using a thin wire thermistor, commonly used for ambient temperature measurement in GPS sonde equipment with a quick response time (shorter than 2 s). The gas temperature change was negligible at the valve change timings between the standard gas and ambient air (< 0.1 K). The result indicated that the gas temperatures were relatively constant after passing through the valves, pump, dehumidifier cell, and piping for both the standard gases and ambient air.

The performances of the CO_2 sonde instruments were checked before the balloon launching since the CO_2 sonde systems were not recovered after the launch experiments were performed. For about 60 min before the launch, the values of $[I\,(4.0) - I\,(4.3)]\,/\,P$ were measured with the valve cycles (each step 40 s, total 160 s) for two standard gas packages ($\sim$ 370 and $\sim$ 400 ppm) for calibration and one intermediate concentration gas package ($\sim$ 385 ppm) as a simulated ambient gas sample.

2.4 Total sonde system

The CO_2 sonde was equipped with a GPS radiosonde (Meisei Electric co., Ltd., RS-06G). The balloon carried the instrument packages in the altitude with measuring CO_2 and meteorological data (GPS position and time, temperature, pressure, and humidity). The CO_2 sonde transmitted those data

to a ground receiver (Meisei Electric co., Ltd., RD-08AC) at 1 s intervals, and thus it was unnecessary to recover the CO_2 sonde after the balloon burst. Figure 2 showed an overall view of the CO_2 sonde developed in this study, which consisted of a CO_2 measurement package, a calibration gas package, a GPS radiosonde, a balloon, and a parachute. The total weight of the CO_2 sonde was 1700 g, including the GPS radiosonde (150 g), CO_2 measurement package (1000 g), and calibration gas package (550 g). The dimensions of the CO_2 measurement package were width (W) 280 mm × height (H) 150 mm × depth (D) 280 mm. The size of the calibration gas package was W 400 mm × H 420 mm × D 490 mm.

The CO_2 sonde system was flown by a 1200 g rubber balloon (Totex). The ascending speed was around 4 m s^{-1} by controlling the helium gas amount in the rubber balloon and checking the buoyancy force. In practice, it was difficult to precisely control the ascending speed of the balloon, and the actual resulting speeds were in the range of 3–5 m s^{-1}. This corresponds to the height resolution of approximately 240–400 m for the measurements of the CO_2 vertical profiles.

Ascending speed slower than 3 m s^{-1} can lead to a collision with a nearby tree and building, resulting in equipment falling in the urban areas. With faster ascending speeds, the altitude resolution of the measurements decreased, the standard gas bag became full, and the pressure inside the gas bags became higher than the ambient pressure because of the lower ambient pressures at higher altitudes. The high pressure inside the gas bag resulted in the fast flow speed in the optical absorption cell of NDIR, which shifted the signal values for the pressurized gas sample. Since pressure relief valves for the bags did not work at low pressures at high altitudes, we did not use the pressure relief valve for the standard gas bags. When the ascending speed was low, the standard gas bags became empty since they were consumed by the in-flight calibration procedures during the long ascending time. Since the measurements after the over-pressurization or the exhaustion of the reference gas bag are useless, this technical problem determines the upper limit (10 km) of altitude for the measurements in this study. Based on our experiences, this problem generally occurred at an altitude above approximately 10 km. A prototype of the CO_2 sonde is available from Meisei Co. Ltd. (Isesaki, Japan) for about USD 4500.

2.5 Data processing procedures

Since the surrounding conditions of the sonde change significantly during the ascending period, the NDIR measurement system is calibrated with the two standard gases at every altitude. However, since the balloon-borne instrument is only equipped with one NDIR absorption cell and the balloon ascends continuously, it is not possible to measure the ambient air sample and the two standard gases at the same time and at the same altitude. Therefore, the measurement cycle during the flights consisted of the following steps: (1) low concentration standard gas, (2) ambient air, (3) high concentration standard gas, and (4) ambient air. The measurement time for each step was 40 s. At switching timings of the valve cycles, the signal became stable within 10 s, and the averages of residual 30 s period signals were used for the calculation of the CO_2 mole fractions. Since the gas exit port of the NDIR optical absorption cell was opened to the ambient air, the cell pressure was equalized with the ambient pressure. During the period of the 40 s gas change, the pressure would change about 2 % when the ascending speed of the balloon was 4 m s^{-1}. The temperature of the ambient air and standard gas samples at the inlet port of the optical cells was measured and found to be constant during each cycle of the calibration procedure.

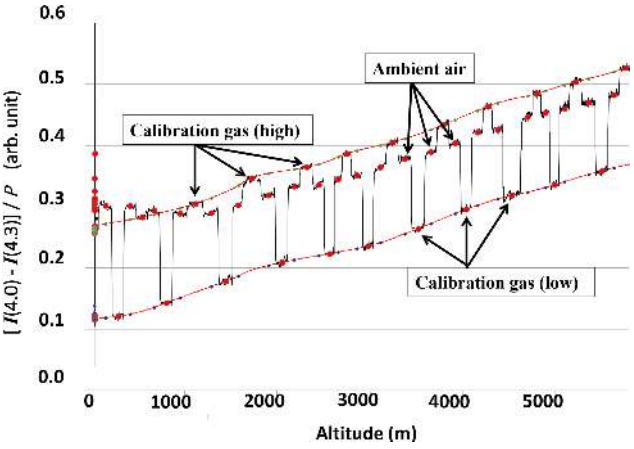

Figure 3. Raw data obtained by the CO_2 sonde launched on 26 September 2011 at Moriya, Japan. The vertical axis is the difference between the 4.0 and 4.3 µm signal intensities divided by the ambient pressure. The black line indicates the observation results during the balloon flight with calibration cycles. The red circle indicates the 30 s average values in each step of the calibration. The red curve indicates the cubic spline fitting curves for the observation points of the 30 s average values of the same standard gas. The small black dots on the cubic spline curves indicate the estimated values for the standard gases at the ambient gas measuring timing, which is used for the interpolation to determine the ambient air concentrations.

Figure 3 shows an example of the raw data obtained from the CO_2 sonde experiment. Figure 3 presents the plots of the values of $[I\,(4.0) - I\,(4.3)]\,/\,P$ against the altitude, where $I\,(4.0)$ and $I\,(4.3)$ are the signal intensities at the wavelength of 4.0 µm for background measurements and the 4.3 µm wavelength for CO_2 absorption measurements, as obtained by the NDIR CO_2 sensor on the balloon, and P is the ambient atmospheric pressure obtained by the GPS sonde data and pressure measurements on the ground.

The values of $[I\,(4.0) - I\,(4.3)]\,/\,P$ are proportional to the CO_2 mole fraction X according to the Beer–Lambert law as expressed by Eq. (2). By using the values of $[I\,(4.0) - I\,(4.3)]\,/\,P$, we can compensate for the pressure change to determine the CO_2 concentration. As shown in

Fig. 3, the differences in the $[I\,(4.0) - I\,(4.3)]\,/\,P$ values between the low and high standard gases remained relatively constant while ascending to the higher altitudes. However, the $[I\,(4.0) - I\,(4.3)]\,/\,P$ values for each standard gas did not change linearly but sometimes displayed some curvatures as shown in Fig. 3. This may be due to the differences between the baseline drifts of the two sensors at 4.3 and 4.0 µm in the NDIR detector. Since the measurements were performed alternately for the standard gases and the ambient air with the NDIR cell and are not performed simultaneously, the values for the standard gas signals at the time of the ambient air measurement were estimated. Therefore, the cubic spline fitting curves for the observation points of the 30 s average values (red circles in Fig. 3) of the same standard gas were used to obtain the low and high calibration points for the calculation of the mole fractions in the ambient air. In Fig. 3, the cubic spline fitting curves are represented by the red curves, and the estimated values for the standard gases at the ambient gas measuring time are represented by the small black dots on the cubic spline curves, which are used for the interpolation to determine the ambient air concentrations. Linear line fitting between the standard gas values did not work well because the connection lines of the values sometimes displayed curvatures as shown in Fig. 3. Since there were in-phase fluctuations in the $I\,(4.0)$ and $I\,(4.3)$ signals during the flights, the subtraction of $[I\,(4.0) - I\,(4.3)]$ could partly improve the signal-to-noise ratios by canceling in-phase fluctuations with each other.

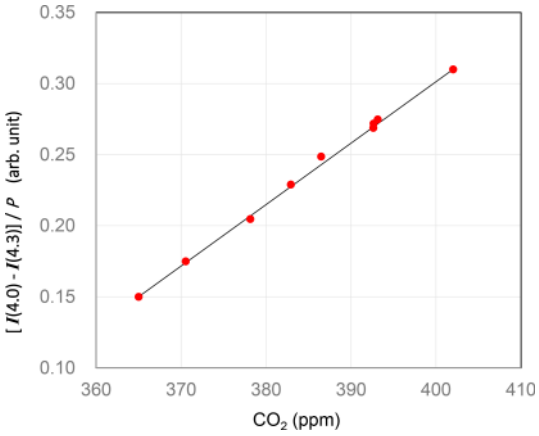

Figure 4. $[I\,(4.0) - I\,(4.3)]\,/\,P$ values versus CO_2 mole fraction, where $I\,(4.0)$ and $I\,(4.3)$ are the signal intensities at the 4.0 µm wavelength for background measurements and the 4.3 µm wavelength for CO_2 absorption measurements, obtained by the NDIR CO_2 sensor, and P is the ambient atmospheric pressure. CO_2 mole fractions were measured with a standard NDIR instrument (LICOR, LI-840A) connected to the balloon sensor in series. The pressure while carrying out the measurements was constant at 1010 hPa.

3 Results and discussion

3.1 Laboratory tests

Since the linear interpolation method for the $[I\,(4.0) - I\,(4.3)]\,/\,P$ values was used to determine the ambient air CO_2 mole fractions in the balloon-borne experiments, the deviations from the linear interpolation process were also investigated. The measurements of various mole fraction gas samples in the laboratory indicated that the linear interpolation error with the two standard gas packages ($\sim$ 370 and $\sim$ 400 ppm) was less than 0.2 ppm in the range between 360 and 410 ppm. Figure 4 shows the measurement results of the NDIR cell developed in this study at various CO_2 mole fractions. The outlet port of the NDIR system was connected to the commercial CO_2 instrument (LICOR, LI-840A) as a standard device, and the two instruments simultaneously measure the sample gas at 1010 hPa. The standard gases of 365 and 402 ppm were used for the calibration, and the mixtures of the standard gases were used for the samples. This indicated the values of $[I\,(4.0) - I\,(4.3)]\,/\,P$ of the system were proportional to the mole fraction of CO_2. This type of experiment could not be performed at low pressures, since we did not have a standard device which can be operated under low pressures.

Figure 5 shows the results of an experiment using a vacuum chamber in the laboratory, where the flight pressure conditions were simulated and the performances of the CO_2 sonde instruments were evaluated. The temperature inside the chamber was not controlled and was about 298 K. In the actual flights, the temperature inside the sonde package did not change more than 5 K. The CO_2 sonde system and two standard gas packages were placed in the vacuum chamber. The chamber was filled with the mole fraction sample gas of 377.3 ppm before the pumping. The pressure of the chamber was gradually and continuously decreased using a mechanical pump from 1010 hPa (ground surface pressure) to 250 hPa (about 10 km altitude pressure) over 60 min, corresponding to a balloon ascending speed of 3 m s^{-1} in actual flights, whereas the sample gas was slowly and continuously supplied to the chamber. The values $[I\,(4.0) - I\,(4.3)]\,/\,P$ were measured for the two standard gas packages and the sample gas with the valve cycles (each step 40 s, total 160 s) as described in the previous section. The mole fractions of the sample gas in the chamber were calculated by the interpolation of the signals for the two standard gases. The 30 s signals 10 s after the valve changes were used for the interpolation calculations to avoid the incomplete gas exchanges in the NDIR optical cell. The black circle in Fig. 5 indicates the sample gas mole fraction obtained from the linearly interpolated standard gas signals in each calibration cycle. The vertical error bar in Fig. 5 indicates the square root of the sum of squares for the standard deviations of the sample and standard gas signals at each step. The errors in the CO_2 mole fractions were estimated to be 0.6 ppm at 1010 hPa and 1.2 ppm at 250 hPa using the calibration cycles. The results in Fig. 5

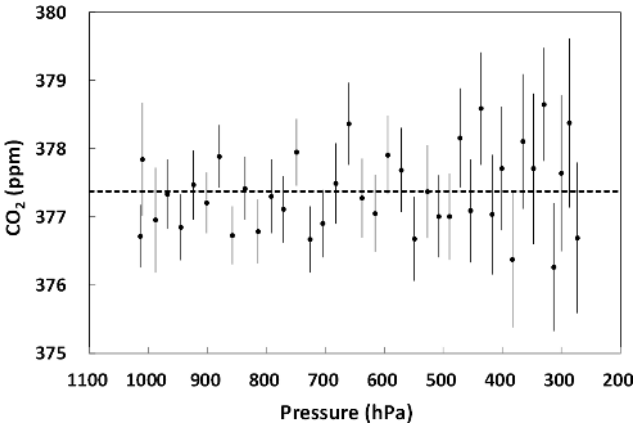

Figure 5. Results of a chamber experiment of the CO_2 sonde. Pressure in the chamber was reduced from 1010 hPa (ground level pressure) to 250 hPa (about 10 km altitude pressure) at a temperature of about 298 K. The black circles indicate the value of the CO_2 mole fraction of the sample air in the chamber, which was obtained from the interpolation of the standard gas values in each calibration cycle. Vertical error bars indicate the square root of the sum of squares for the standard deviations of the sample and standard gas signals at each step in the calibration cycle. The black dashed line shows an average of all the values obtained for the sample gas. See the text for more details.

indicated that the determination of the sample gas concentration using the linear interpolation with the standard gases was appropriate within the error, when the pressure continuously decreased from 1000 to 250 ppm over 60 min.

When the CO_2 sonde instrument was inclined and vibrated in the laboratory, the fluctuations in the signals were observed. The quantitative correlation between the signal fluctuation intensities and acceleration speed, measured by a three-dimensional acceleration sensor, was investigated, but no distinct correlation was detected. However, the in-flight calibration system partly solved this problem by taking the signal difference of $[I\,(4.0) - I\,(4.3)]$ and also by measuring alternately the two standard gases every 40 s during the balloon flights.

The temperature characteristics of the CO_2 sensor were also investigated by changing the sensor cell block temperature from 273 to 323 K at the pressure of $\sim$ 1010 hPa, using a heater in the laboratory. The laboratory experiment related to the temperature dependence suggested that the measurement error is less than 0.2 ppm due to the temperature change during one valve cycle (160 s) in the balloon-borne experiments.

In principle, the absorption intensities $(I_0 - I)$ in the NDIR measurements are proportional to the absolute CO_2 concentrations in the sample air in the absorption cell. Therefore, at higher altitudes where the pressures were lower, the values of $[I\,(4.0) - I\,(4.3)]$ were smaller and the signal-to-noise ratios decreased. The error of the CO_2 mole fractions of 1.2 ppm at 250 hPa corresponds to an absolute CO_2 concentration of 3.2×10^{13} molecule cm^{-3}. The equivalent altitude for this value was 90 km with a CO_2 molar fraction of 400 ppm. As described previously, the purpose of CO_2 balloon observations is to measure the CO_2 mole fraction within 1 ppm errors in the atmospheres around 400 ppm CO_2. The upper limit of the altitude for the observations with the developed CO_2 sonde is considered to be $\sim$ 10 km. Furthermore, as described in Sect. 2.4, the problems of the vacancy or overpressure in the standard gas bags took place around 10 km altitudes, which resulted in large errors. This also practically determines the upper altitude limit for CO_2 sonde observations.

3.2 Comparison with aircraft data

Two types of aircraft measurement data, the NIES/JAXA chartered aircraft and the CONTRAIL data, were used for comparison with the CO_2 sonde measurement data. The NIES/JAXA chartered aircraft measurements were conducted on the same days as the CO_2 sonde observations (31 January and 3 February 2011). The chartered aircraft observations were performed as a part of the campaign for validating the GOSAT data and calibrating the TCCON FTS data at Tsukuba (36.05° N, 140.12° E) (Tanaka et al., 2012). The chartered aircraft data were obtained using an NDIR instrument (LICOR LI-840) that had a control system of constant pressure and had the uncertainty of 0.2 ppm. On both 31 January and 3 February, the chartered aircraft measured the CO_2 mole fractions during descent spirals over Tsukuba and Kumagaya (Fig. 6). Because the air traffic was strictly regulated near Haneda and Narita international airports, the aircraft observations at altitudes above 2 km over Tsukuba were prohibited. Therefore, the descent spiral observations were conducted over Kumagaya at altitudes of 7–2 km and over Tsukuba at altitudes of 2–0.5 km. Tsukuba is located approximately 20 km northeast of Moriya, whereas Kumagaya is located approximately 70 km northwest of Moriya.

Seven profiles based on the CONTRAIL measurements, obtained during the ascent and descent of aircrafts over Narita airport and with passage times close to the CO_2 sonde observations, were available within 2 d after or before the dates of the CO_2 sonde measurements (Table 1). The CO_2 sonde observations were conducted on 31 January and 3 February 2011 from Moriya. One set of CONTRAIL data, obtained from the flight from Hong Kong to Narita (data set name: 11_060d), was available on 31 January, but no CONTRAIL data were available for 3 February. Therefore, the CONTRAIL data, obtained from the flight from Hong Kong to Narita on 2 February (data set name: 11_062d), were used for comparison with the 3 February CO_2 sonde data. Figure 6 also shows the CONTRAIL 11_060d and 11_062d flight paths and the CO_2 sonde launched at Moriya on 31 January and 3 February 2011. On 31 January the flight time of the CONTRAIL 11_060d over Narita airport and the launch time of the CO_2 sonde at Moriya were relatively close to one another. The flight path of the CONTRAIL 11_062d data

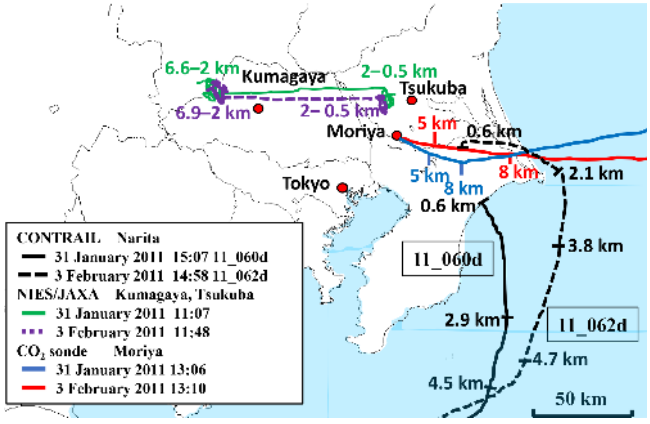

Figure 6. Flight paths of the CO_2 sonde observations launched at Moriya on 31 January (blue solid line) and 3 February (red solid line) 2011, the CONTRAIL 11_060d data on 31 January 2011 (black solid line) and 11_062d data on 2 February 2011 (black dashed line) from Hong Kong to Narita, and the NIES/JAXA chartered aircraft experiment on 31 January (green solid line) and 3 February (purple dotted line). The altitudes of the flight paths are also indicated.

Table 1. CONTRAIL flight data near to the CO_2 sonde measurements on 31 January and 3 February 2011.

Data set name	Date	Time (LST)*
11_057a	CONTRAIL (29 January)	19:01
11_058d	CONTRAIL (30 January)	15:06
11_059a	CONTRAIL (30 January)	18:46
11_060d	CONTRAIL (31 January)	15:07
11_061a	CONTRAIL (1 February)	18:46
11_062d	CONTRAIL (2 February)	14:58
11_063a	CONTRAIL (4 February)	18:58
	CO_2 sonde (31 January)	13:06
	CO_2 sonde (3 February)	13:10

* Time for the CONTRAIL data represents the flight time in Japan Standard Time at an altitude of 1 km over Narita airport. Time for the CO_2 sonde data represents the launching time at Moriya.

on 2 February 2011 was close to that of the CO_2 sonde on 3 February 2011, and both observations were conducted in the early afternoon. The CONTRAIL data referred to in the present study were obtained using the Continuous CO_2 Measuring Equipment (CME) located onboard commercial airliners (Machida et al., 2008; Matsueda et al., 2008). The typical measurement uncertainty (1σ) of the CME has been reported as 0.2 ppm (Machida et al., 2008).

Figure 7 shows the vertical profiles of CO_2 observed by the CO_2 sonde at Moriya, the chartered aircraft at Kumagaya and Tsukuba, and the CONTRAIL over Narita airport on 31 January 2011. The overall vertical distribution of the CO_2 sonde data resembled those of the chartered aircraft. The vertical profiles of the CONTRAIL 11_060d flight on 31 January at

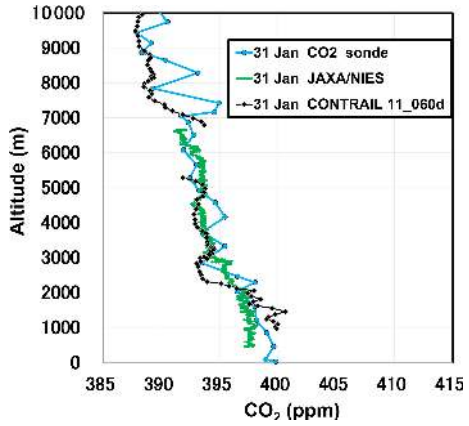

Figure 7. The CO_2 vertical profiles obtained by the CO_2 sonde (circles connected with blue lines), NIES/JAXA chartered aircraft data (dots connected with green lines), and the CONTRAIL data (diamonds connected with black lines) on 31 January 2011.

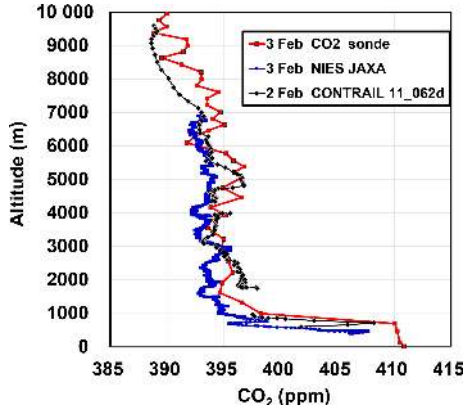

Figure 8. The CO_2 vertical profiles obtained by the CO_2 sonde (circles connected with red lines), NIES/JAXA chartered aircraft data (dots connected with purple lines) on 3 February, and CONTRAIL data (diamonds connected with black lines) on 2 February 2011.

the 5.3–6.8 km altitude range consisted of the missing data because of the CME calibration period.

Figure 8 shows the comparison of the CO_2 vertical profiles obtained by the CO_2 sonde over Moriya, NIES/JAXA chartered aircraft over Kumagaya and Tsukuba on 3 February 2011, and the CONTRAIL on 2 February 2011 over Narita. The shape of the vertical profile obtained by the chartered aircraft on 3 February resembled that obtained by the CO_2 sonde, although the profile from the chartered aircraft was shifted to the lower CO_2 concentration side compared to that of the CO_2 sonde.

Table 2 lists the comparisons of the CO_2 mole fractions measured by the balloon CO_2 sonde and NIES/JAXA chartered aircraft on 31 January and 3 February 2011. The averaged values of the aircraft measurement over the range of each balloon altitude ± 100 m are listed in Table 2, since the altitude resolution of the aircraft measurements is higher than

Table 2. Comparisons of the CO_2 mole fractions between the balloon CO_2 sonde and NIES/JAXA chartered aircraft measurements on 31 January and 3 February 2011.

JAXA-NIES chartered aircraft (31 January 2011)				JAXA-NIES chartered aircraft (3 February 2011)			
Altitude (m)[a]	Balloon CO_2 (ppm)	Aircraft CO_2 (ppm)[b]	Difference (ppm)[c]	Altitude (m)[a]	Balloon CO_2 (ppm)	Aircraft CO_2 (ppm)[b]	Difference (ppm)[c]
849	399.05	397.62	1.43	1324	396.60	394.45	2.15
1202	398.16	397.53	0.63	1612	394.65	393.03	1.62
1610	398.00	397.17	0.83	1917	394.86	394.10	0.76
2038	396.50	396.95	−0.45	2223	395.77	393.54	2.23
2291	398.03	396.04	1.99	2539	395.41	393.95	1.45
2463	396.54	395.65	0.89	2867	394.71	395.11	−0.40
2844	393.44	395.24	−1.79	3215	394.99	392.99	2.00
3329	395.45	394.15	1.30	3543	393.59	393.07	0.52
3732	393.51	393.63	−0.12	3764	393.69	393.40	0.28
4161	395.47	393.54	1.93	3938	395.15	393.11	2.04
4575	394.62	392.94	1.68	4169	393.83	392.68	1.15
4918	393.24	393.64	−0.41	4458	396.57	393.51	3.06
5273	392.41	393.25	−0.84	4750	394.88	393.69	1.19
5654	393.02	393.47	−0.45	5047	396.53	394.01	2.53
6083	391.87	392.91	−1.04	5214	395.91	393.45	2.46
6510	392.76	391.65	1.11	5383	396.78	393.58	3.20
		Average =	0.42	5565	395.83	393.67	2.15
		SD[d] =	1.16	5781	395.18	393.39	1.80
		rms[e] =	1.20	6092	391.75	392.83	−1.09
				6287	392.44	392.42	0.02
				6467	393.67	392.23	1.44
				6639	395.07	392.42	2.65
				6815	394.00	393.00	1.00
						Average =	1.41
						SD[d] =	1.00
						rms[e] =	1.62

[a] Altitudes of the balloon-borne experiments using the in-flight calibration with 40 s time intervals. [b] Averaged values of the aircraft measurement results over the range of the balloon altitudes ±100 m. [c] Difference values of [balloon CO_2] − [aircraft CO_2]. [d] Standard deviation of the differences (1σ). [e] Root mean square values.

that of the CO_2 sonde. From the 3 February measurements, the height of the boundary layer around an altitude of 1 km was different between the CO_2 sonde and the NIES/JAXA aircraft measurements, as shown in Fig. 8. Therefore, the data below 1 km on 3 February are not included in Table 2. From the data on 31 January, the averaged value of the differences between the CO_2 sonde and the NIES/JAXA aircraft was relatively small (0.42 ppm), which corresponded to the bias of the measurements. The standard deviation of the differences was 1.24 ppm. From the 3 February data, the bias was large (1.41 ppm), whereas the standard deviation of the differences was not so large (1.00 ppm), which corresponded to the similar but shifted vertical profiles in shapes between the CO_2 sonde and aircraft measurements as shown in Fig. 8. The difference between the CO_2 sonde data and the NIES/JAXA chartered aircraft data on 3 February is nearly equal to the difference between CONTRAIL data on 2 February and the NIES/JAXA chartered aircraft data on 3 February.

Table 3 lists the comparisons of the CO_2 mole fractions measured by the balloon CO_2 sonde and CONTRAIL aircraft, 11_060d on 31 January and 11_062d on 2 February 2011 up to the altitude of 7000 m. The averaged values of the aircraft measurements over the range of each balloon altitude ±100 m are listed in Table 3. The biases between the CO_2 sonde and the CONTRAIL aircraft results were relatively small, 0.33 and 0.35 ppm, and the standard deviations of the differences were 1.16 and 1.30 ppm for the results on 31 January and 3 February, respectively.

From the comparison between the CO_2 sonde data and the aircraft (NIES/JAXA and CONTRAIL) data, it was found that the CO_2 sonde observation was larger than those of aircrafts by about 0.6 ppm on average. The standard deviation of the difference from the CO_2 sonde and aircraft observations was 1.2 ppm (1σ). If the four sets of aircraft measurement data obtained by the NIES/JAXA and CONTRAIL observations were accurate within the published uncertainties, ignoring the differences in the flight time and geographical

Table 3. Comparisons of the CO_2 mole fractions between the balloon CO_2 sonde measurements on 31 January and CONTRAIL aircraft CME on 31 January (11_060d) and between the CO_2 sonde on 3 February and CONTRAIL on 2 February (11_062d) up to the altitude of 7 km. The annotations are the same as Table 2.

CONTRAIL 11_060d (31 January 2011)				CONTRAIL 11_062d (2 February 2011)			
Altitude (m)	Balloon CO_2 (ppm)	Aircraft CO_2 (ppm)	Difference (ppm)	Altitude CO_2 (m)	Balloon CO_2 (ppm)	Aircraft (ppm)	Difference (ppm)
849	399.05	398.21	0.84	1917	394.86	396.59	−1.73
1202	398.16	399.56	−1.40	2223	395.77	396.45	−0.68
1610	398.00	398.77	−0.76	2539	395.41	395.71	−0.30
2038	396.50	397.07	−0.57	2867	394.71	394.67	0.04
2291	398.03	395.97	2.06	3215	394.99	393.34	1.65
2463	396.54	394.55	1.99	3543	393.59	394.25	−0.66
2844	393.44	393.41	0.04	3764	393.69	394.33	−0.64
3329	395.45	394.25	1.20	3938	395.15	394.69	0.46
3732	393.51	393.58	−0.07	4458	396.57	394.09	2.48
4161	395.47	393.86	1.61	4750	394.88	395.02	−0.14
4575	394.62	393.18	1.44	5047	396.53	396.55	−0.01
4918	393.24	393.62	−0.38	5214	395.91	396.01	−0.10
5273	392.41	392.76	−0.35	5383	396.78	394.78	2.00
6866	392.31	393.26	−0.96	5565	395.83	393.69	2.14
		Average =	0.33	5781	395.18	393.79	1.39
		SD =	1.16	6092	391.75	393.57	−1.82
		rms =	1.17	6287	392.44	393.32	−0.88
				6467	393.67	392.89	0.78
				6639	395.07	392.84	2.23
				6815	394.00	393.11	0.90
						Average =	0.35
						SD =	1.30
						rms =	1.31

routes, the measurement error of the CO_2 sonde system was estimated from the standard deviations of all the difference values in Tables 2 and 3. The estimated error value up to an altitude of 7 km was 0.6 ± 1.2 ppm for the CO_2 sonde observation with a 240 m altitude resolution and 3 m s^{-1} ascending speed. The root mean square value (1.3 ppm) from all the difference values in Tables 2 and 3 indicated that the CO_2 sonde could measure the CO_2 vertical profiles within 1.3 ppm on average compared to the aircraft observations. It is noted that, although error estimation was conducted for the data up to an altitude of 7 km due to the availability of the chartered aircraft data, the CO_2 sonde data above 7 km up to about 10 km were available. The measurement errors for the data above 7 km are expected to be larger than the above estimation.

3.3 CO_2 sonde observations over a forested area

Figure 9 shows the vertical profiles of the CO_2 mole fraction, temperature, and relative humidity obtained from the balloon-borne experiments of the CO_2 sonde at Moshiri (44.4° N, 142.3° E) on 26 August 2009. The launch site is in a rural area of Hokkaido, Japan, and is surrounded by forests. The CO_2 sonde was launched at 13:29 LST and ascended with a mean vertical speed of approximately 3 m s^{-1}. The CO_2 sonde reached an altitude of 10 km after 56 min. The wind horizontally transported the CO_2 sonde distances of 10 and 21 km northeast when the CO_2 sonde reached the altitudes of 5 and 8 km, respectively. The CO_2 sonde rapidly moved 52 km southeast at an altitude of 16 km. Finally, the CO_2 sonde reached an altitude of 28 km before the balloon burst and the subsequent fall of the sonde was directed by the parachute into the Sea of Okhotsk located 80 km east of the launch site. The error bars for the CO_2 mole fraction in Fig. 9a were calculated from the deviation of the signal intensities from the CO_2 sensor during the 40 s measurement periods for the ambient air and the two standard gases.

The vertical temperature profile in Fig. 9b indicated the existence of three inversion layers of the altitudes of approximately 2.0, 3.2, and 4.3 km. The relative humidity from the ground to the first inversion layer at 2.0 km and between the second and third inversion layers from 3.2 to 4.3 km was higher compared with that observed from 2.0 to 3.2 and from 4.3 to 7.5 km. The CO_2 mole fraction was lowest near the ground ($\sim$ 373 ppm) and increased to approximately 384 ppm at an altitude of 4–5 km around the third inversion layer before reaching a value of 387 ppm in the upper troposphere (5–9 km). Significant decreases in the CO_2 mole frac-

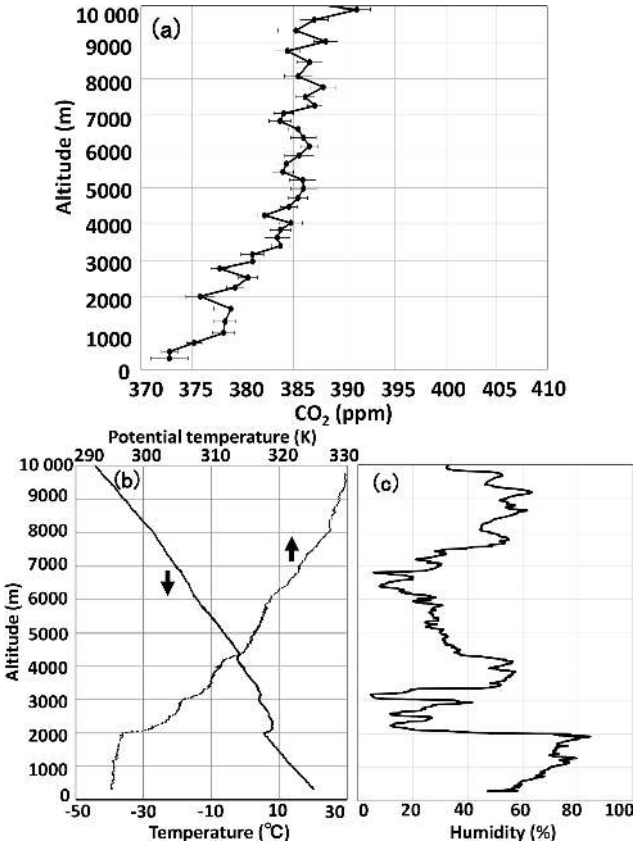

Figure 9. Profiles of **(a)** CO_2 mole fraction, **(b)** temperature (solid line) and potential temperature (dotted line), and **(c)** relative humidity observed over a forest area, Moshiri in Hokkaido, Japan, by the balloon launched on 26 August 2009 at 13:30 (LST). The black circles with error bars in panel **(a)** represent the data obtained by the CO_2 sonde.

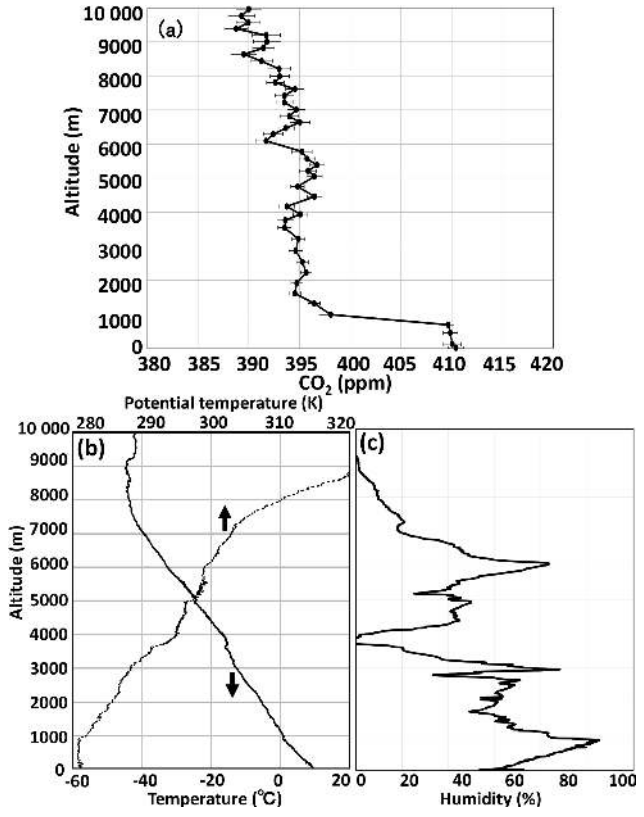

Figure 10. Profiles of **(a)** CO_2 mole fraction, **(b)** temperature (solid line) and potential temperature (dotted line), and **(c)** relative humidity observed over an urban area, Moriya near Tokyo, on 3 February 2011 at 13:10 (LST).

tions were observed in the two lower layers from the ground to 3.2 km. Considering the clear weather on the day of the balloon experiment, these results are explained by the uptake of CO_2 near the surface by plants in the forests through photosynthesis processes in the daytime hours and the diffusion and advection of the air mass containing low CO_2 concentrations at the upper altitudes.

Because the CO_2 mole fraction for the vertical profiles near the surface is critically important to estimating the flux around the observation point, the vertical profile data taken by our CO_2 sonde are useful.

3.4 CO_2 sonde observations over an urban area

Figure 10 shows the vertical profiles of the CO_2 mole fraction, temperature, and relative humidity obtained by the CO_2 sonde at Moriya (35.93° N, 140.00° E) on 3 February 2011. The launching time was 13:10 LST and the sonde ascended with a mean vertical speed of approximately 2.9 m s^{-1}. Moriya is located in the Kanto region and is 40 km northeast of the Tokyo metropolitan area. The launching site was surrounded by the heavy traffic roads and residential areas. As seen in Fig. 10a, high CO_2 mole fractions were observed from the ground up to an altitude of 1 km. The average CO_2 volume mole fraction in this layer was higher than that measured in the free troposphere approximately above 15 ppm. A small temperature inversion layer appeared at approximately 1 km, and the maximum relative humidity was observed just below this inversion layer (Fig. 10b and c). These results suggested that the CO_2 emitted from anthropogenic sources in and/or around the Tokyo metropolitan area accumulated in the boundary layer at altitudes below 1 km.

An analysis of Figs. 9 and 10 indicated that there were a clear local consumption and emission of CO_2 from the comparison of the levels of CO_2 concentration in the free troposphere, which suggested a decoupling with the boundary layer and synoptic inversion layers (Mayfield and Fochesatto, 2013). When a small increase in a column XCO_2 value is observed by a satellite, it is difficult to estimate which part of the atmosphere is responsible for the increase in XCO_2, the boundary layer with strong CO_2 emission in the nearby area, or the free troposphere. Considering this fact, the vertical profile data obtained by the CO_2 sonde around urban ar-

eas should provide more useful information than the column-averaged observations obtained by the satellites and FTS measurements to estimate the flux of anthropogenic CO_2 emitted in and/or around the urban areas.

4 Conclusion

The CO_2 sonde is shown to be a feasible instrument for CO_2 measurements in the troposphere. The laboratory test with a vacuum chamber has shown the precision of the CO_2 sonde at ~ 1010 hPa for 0.6 ppm and at ~ 250 hPa for 1.2 ppm. Comparisons of the CO_2 vertical profiles obtained by the CO_2 sonde with two types of aircraft observations, the CONTRAIL and the NIES/JAXA chartered aircraft, were carried out. The CO_2 sonde and CONTRAIL data were consistent. The CO_2 sonde data on 31 January 2011 were in good agreement with the chartered aircraft data on the same day, but the CO_2 sonde data observed on 3 February 2011 were larger by approximately 1.4 ppm, as compared with the chartered aircraft data obtained on the same day from the ground to an altitude of 7 km. The measurement errors of the CO_2 sonde system up to an altitude of 7 km were estimated to be 1.4 ppm for a single point of 80 s period measurements with a vertical height resolution of 240–400 m. We conducted the field CO_2 sonde observations more than 20 times in Japan and successfully obtained CO_2 vertical profiles from the ground up to altitudes of approximately 10 km.

Our results showed that low-cost CO_2 sondes could potentially be used for frequent measurements of vertical profiles of CO_2 in many parts of the world, providing useful information to understand the global and regional carbon budgets by replenishing the present sparse observation coverage. The CO_2 sondes can detect the local and regional transport evidence by determining CO_2 concentrations in the air layer trapped between elevated inversion layers. Also, the CO_2 sonde observation data could help improve the intercomparison exercise for inverse models and for the partial validation of satellite column integral data. In future, the CO_2 sonde data will be used for the validation of satellites and the calibration of ground-based observations of sunlight spectroscopic measurements for column values of CO_2 concentration.

Data availability. The CO_2 sonde and chartered aircraft data used in this paper are available on request to the corresponding author. The CONTRAIL CME CO_2 data are available on the Global Environmental Database of the Center for Global Environmental Studies at the National Institute for Environmental Studies (https://doi.org/10.17595/20180208.001, Machida et al., 2018).

Author contributions. MO, YM, TN, KS, and TS developed the CO_2 sonde and conducted laboratory experiments and field observations with contributions of RI. TM, HM, YS, IS, OU, and TT obtained the CONTRAIL and chartered aircraft data for the validation of CO_2 sonde. MO, YM, and TN analyzed data and prepared the manuscript with contributions of all of the other authors.

Competing interests. The authors declare that they have no conflict of interest.

Acknowledgements. We would like to thank Noriji Toriyama, Masahiro Kanada, Hidehiko Jindo, Masayuki Sera, Hiroshi Sasago, Tomoyuki Ide, Shoichiro Takekawa, Masahiro Kawasaki, Gen Inoue (Nagoya Univ.), Masatomo Fujiwara, Yoichi Inai (Hokkaido Univ.), Shuji Aoki, and Takakiyo Nakazawa (Tohoku Univ.) for their assistance and useful suggestions in the development of the CO_2 sonde and the observations.

Financial support. This research has been supported by the Grant-in-Aid for Scientific Research (grant nos. KAKENHI 20310008 and KAKENHI 24310012), the Green Network of Excellence, Environmental Information (GRENE-ei) program from the Ministry of Education, Culture, Sports, Science and Technology (MEXT), the Development of Systems and Technology for Advanced Measurement and Analysis Program from the Japan Science and Technology Agency (JST), and the joint research program of the Solar-Terrestrial Environment Laboratory (now new organization: the Institute for Space-Earth Environmental Research), Nagoya University.

Review statement. This paper was edited by Christof Janssen and reviewed by four anonymous referees.

References

Ahmadov, R., Gerbig, C., Kretschmer, R., Körner, S., Rödenbeck, C., Bousquet, P., and Ramonet, M.: Comparing high resolution WRF-VPRM simulations and two global CO_2 transport models with coastal tower measurements of CO_2, Biogeosciences, 6, 807–817, https://doi.org/10.5194/bg-6-807-2009, 2009.

Andrews, A. E., Kofler, J. D., Trudeau, M. E., Williams, J. C., Neff, D. H., Masarie, K. A., Chao, D. Y., Kitzis, D. R., Novelli, P. C., Zhao, C. L., Dlugokencky, E. J., Lang, P. M., Crotwell, M. J., Fischer, M. L., Parker, M. J., Lee, J. T., Baumann, D. D., Desai, A. R., Stanier, C. O., De Wekker, S. F. J., Wolfe, D. E., Munger, J. W., and Tans, P. P.: CO_2, CO, and CH_4 measurements from tall towers in the NOAA Earth System Research Laboratory's Global Greenhouse Gas Reference Network: instrumentation, uncertainty analysis, and recommendations for future high-accuracy greenhouse gas monitoring efforts, Atmos. Meas. Tech., 7, 647–687, https://doi.org/10.5194/amt-7-647-2014, 2014.

Baker, D. F., Law, R. M., Gurney, K. R., Rayner, P., Peylin, P., Denning, A. S., Bousquet, P., Bruhwiler, L., Chen, Y.-H., Ciais, P., Fung, I. Y., Heimann, M., John, J., Maki, T., Maksyutov, S., Masarie, K., Prather, M., Pak, B., Taguchi, S., and Zhu, S.: TransCom 3 inversion intercomparison: Impact of trans-

port model errors on the interannual variability of regional CO_2 fluxes, 1988–2003, Global Biogeochem. Cy., 20, GB1002, https://doi.org/10.1029/2004GB002439, 2006.

Bakwin, P. S., Tans, P. P., Zhao, C., Ussler III, W., and Quesnell, E.: Measurements of carbon dioxide on a very tall tower, Tellus B, 47, 535–549, https://doi.org/10.1034/j.1600-0889.47.issue5.2.x, 2002.

Chédin, A., Serrar, S., Armante, R., Scott, N. A., and Hollingsworth, A.: Signatures of annual and seasonal variations of CO_2 and other greenhouse gases from comparisons between NOAA TOVS observations and radiation model simulations, J. Climate, 15, 95–116, https://doi.org/10.1175/1520-0442(2002)015<0095:SOAASV>2.0.CO;2, 2002.

Conway, T. J., Tans, P. P., Waterman, L. S., Thoning, K. W., Masarie, K. A., and Gammon, R. H.: Atmospheric carbon dioxide measurements in the remote global troposphere, 1981–1984, Tellus B, 40, 81–115, https://doi.org/10.1111/j.1600-0889.1988.tb00214.x, 1988.

Conway, T. J., Tans, P. P., Waterman, L. S., Thoning, K. W., Kitzis, D. R., Masarie, K. A., and Zhang, N.: Evidence for interannual variability of the carbon cycle from the National Oceanic and Atmospheric Administration/Climate Monitoring and Diagnostics Laboratory global air sampling network, J. Geophys. Res., 99, 22831–22855, https://doi.org/10.1029/94JD01951, 1994.

Crevoisier, C., Heilliette, S., Chédin, A., Serrar, S., Armante, R., and Scott, N. A.: Midtropospheric CO_2 concentration retrieval from AIRS observations in the tropics, Geophys. Res. Lett., 31, L17106, https://doi.org/10.1029/2004GL020141, 2004.

Daube, B. C., Boering, K. A., Andrews, A. E., and Wofsy, S. C.: A high-precision fast-response airborne CO_2 analyzer for in situ sampling from the surface to the middle stratosphere, J. Atmos. Ocean. Tech., 19, 1532–1543, https://doi.org/10.1175/1520-0426(2002)019<1532:AHPFRA>2.0.CO;2, 2002.

Dils, B., De Mazière, M., Müller, J. F., Blumenstock, T., Buchwitz, M., de Beek, R., Demoulin, P., Duchatelet, P., Fast, H., Frankenberg, C., Gloudemans, A., Griffith, D., Jones, N., Kerzenmacher, T., Kramer, I., Mahieu, E., Mellqvist, J., Mittermeier, R. L., Notholt, J., Rinsland, C. P., Schrijver, H., Smale, D., Strandberg, A., Straume, A. G., Stremme, W., Strong, K., Sussmann, R., Taylor, J., van den Broek, M., Velazco, V., Wagner, T., Warneke, T., Wiacek, A., and Wood, S.: Comparisons between SCIAMACHY and ground-based FTIR data for total columns of CO, CH_4, CO_2 and N_2O, Atmos. Chem. Phys., 6, 1953–1976, https://doi.org/10.5194/acp-6-1953-2006, 2006.

Durry, G., Amarouche, N., Zéninari, V., Parvitte, B., Lebarbu, T., and Ovarlez, J.: In situ sensing of the middle atmosphere with balloon borne near-infrared laser diodes, Spectrochim. Acta A, 60, 3371–3379, https://doi.org/10.1016/j.saa.2003.11.050, 2004.

Eldering, A., O'Dell, C. W., Wennberg, P. O., Crisp, D., Gunson, M. R., Viatte, C., Avis, C., Braverman, A., Castano, R., Chang, A., Chapsky, L., Cheng, C., Connor, B., Dang, L., Doran, G., Fisher, B., Frankenberg, C., Fu, D., Granat, R., Hobbs, J., Lee, R. A. M., Mandrake, L., McDuffie, J., Miller, C. E., Myers, V., Natraj, V., O'Brien, D., Osterman, G. B., Oyafuso, F., Payne, V. H., Pollock, H. R., Polonsky, I., Roehl, C. M., Rosenberg, R., Schwandner, F., Smyth, M., Tang, V., Taylor, T. E., To, C., Wunch, D., and Yoshimizu, J.: The Orbiting Carbon Observatory-2: first 18 months of science data products, Atmos. Meas. Tech., 10, 549–563, https://doi.org/10.5194/amt-10-549-2017, 2017.

Fang, S. X., Zhou, L. X., Tans, P. P., Ciais, P., Steinbacher, M., Xu, L., and Luan, T.: In situ measurement of atmospheric CO_2 at the four WMO/GAW stations in China, Atmos. Chem. Phys., 14, 2541–2554, https://doi.org/10.5194/acp-14-2541-2014, 2014.

Galais, A., Fortunato, G., and Chavel, P: Gas concentration measurement by spectral correlation: rejection of interferent species, Appl. Optics, 24, 2127–2134, https://doi.org/10.1364/ao.24.002127, 1985.

Gurney, K. R., Law, R. M., Denning, A. S., Rayner, P. J., Baker, D., Bousquet, P., Bruhwiler, L., Chen, Y. -H., Ciais, P., Fan, S., Fung, I. Y., Gloor, M., Heimann, M., Higuchi, K., John, J., Maki, T., Maksyutov, S., Masarie, K., Peylin, P., Prather, M., Pak, B. C., Randerson, J., Sarmiento, J., Taguchi, S., Takahashi, T., and Yuen, C.-W.: Towards robust regional estimates of CO_2 sources and sinks using atmospheric transport models, Nature, 415, 626–630, https://doi.org/10.1038/415626a, 2002.

Gurney, K. R., Law, R. M., Denning, A. S., Rayner, Pak, B., Baker, D. F., Bousquet, P., Bruhwiler, L. M. P., Chen, Y. -H., Ciais, P., Fung, I. Y., Heimann, M., John, J. G., Maki, T., Maksyutov, S., Peylin, P., Prather, M. J., and Taguchi, S.: Transcom 3 inversion intercomparison: Model mean results for the estimation of seasonal carbon sources and sinks, Global Biogeochem. Cy., 18, GB1010, https://doi.org/10.1029/2003GB002111, 2004.

Ghysels, M., Durry, G., Amarouche, N., Cousin, J., Joly, L., Riviere, E. D., and Beaumont, L.: A lightweight balloon-borne laser diode sensor for the in situ measurement of CO_2 at 2.68 micron in the upper troposphere and the lower stratosphere, Appl. Phys. B, 107, 213–220, https://doi.org/10.1007/s00340-012-4887-y, 2012.

Hodgkinson, J., Smith, R., Ho, W. O., Saffell, J. R., and Tatam, R. P.: Non-dispersive infra-red (NDIR) measurement of carbon dioxide at 4.2 µm in a compact and optically efficient sensor, Sensor. Actuat. B-Chem., 186, 580–588, https://doi.org/10.1016/j.snb.2013.06.006, 2013.

Inai, Y., Aoki, S., Honda, H., Furutani, H., Matsumi, Y., Ouchi, M., Sugawara, S., Hasebe, F., Uematsu, M., and Fujiwara, M.: Balloon-borne tropospheric CO_2 observations over the equatorial eastern and western Pacific, Atmos. Environ., 184, 24–36, https://doi.org/10.1016/j.atmosenv.2018.04.016, 2018.

Inoue, H. Y. and Matsueda, H.: Measurements of atmospheric CO_2 from a meteorological tower in Tsukuba, Japan, Tellus B, 53, 205–219, https://doi.org/10.1034/j.1600-0889.2001.01163.x, 2001.

Joly, L., Parvitte, B., Zeninari, V., and Durry, G.: Development of a compact CO_2 sensor open to the atmosphere and based on near-infrared laser technology at 2.68 µm, Appl. Phys. B, 86, 743–748, https://doi.org/10.1007/s00340-006-2568-4, 2007.

Karion, A., Sweeney, C., Tans, P., and Newberger, T.: AirCore: An innovative atmospheric sampling system, J. Atmos. Ocean. Tech., 27, 1839–1853, https://doi.org/10.1175/2010JTECHA1448.1, 2010.

Komhyr, W. D., Harris, T. B., Waterman, L. S., Chin, J. F. S., and Thoning, K. W.: Atmospheric carbon dioxide at Mauna Loa Observatory 1. NOAA global monitoring for climatic change measurements with a nondispersive infrared analyzer, 1974–1985, J. Geophys. Res., 94, 8533–8547, https://doi.org/10.1029/JD094iD06p08533, 1989.

Machida, T., Matsueda, H., Sawa, Y., Nakagawa, Y., Hirotani, K., Kondo, N., Goto, K., Ishikawa, K., Nakazawa, T., and Ogawa, T.:

Worldwide measurements of atmospheric CO_2 and other trace gas species using commercial airlines, J. Atmos. Ocean. Tech., 25, 1744–1754, https://doi.org/10.1175/2008JTECHA1082.1, 2008.

Machida, T., Matsueda, H., Sawa, Y., and Niwa, Y.: Atmospheric CO_2 mole fraction data of CONTRAIL-CME, Center for Global Environmental Research, NIES, https://doi.org/10.17595/20180208.001, 2018.

Maksyutov, S., Nikolay, K., Nakatsuka, Y., Patra, P. K., Nakazawa, T., Yokota, T., and Inoue, G.: Projected Impact of the GOSAT observations on regional CO_2 flux estimations as a function of total retrieval error, J. Remote Sensing Soc. Japan, 28, 190–197, https://doi.org/10.11440/rssj.28.190, 2008.

Matsueda, H., Machida, T., Sawa, Y., Nakagawa, Y., Hirotani, K., Ikeda, H., Kondo, N., and Goto, K.: Evaluation of atmospheric CO_2 measurements from new flask air sampling of JAL airliner observations, Pap. Meteorol. Geophys., 59, 1–17, https://doi.org/10.2467/mripapers.59.1, 2008.

Mayfield, J. A. and Fochesatto, G. J.: The Layered Structure of the winter Atmospheric Boundary Layer in the Interior of Alaska, J. Appl. Meteorol. Clim., 52, 953–973, https://doi.org/10.1007/s00703-013-0274-4, 2013.

Morino, I., Uchino, O., Inoue, M., Yoshida, Y., Yokota, T., Wennberg, P. O., Toon, G. C., Wunch, D., Roehl, C. M., Notholt, J., Warneke, T., Messerschmidt, J., Griffith, D. W. T., Deutscher, N. M., Sherlock, V., Connor, B., Robinson, J., Sussmann, R., and Rettinger, M.: Preliminary validation of column-averaged volume mixing ratios of carbon dioxide and methane retrieved from GOSAT short-wavelength infrared spectra, Atmos. Meas. Tech., 4, 1061–1076, https://doi.org/10.5194/amt-4-1061-2011, 2011.

Nakazawa, T., Murayama, S., Miyashita, K., Aoki, S., and Tanaka, M.: Longitudinally different variations of lower tropospheric carbon dioxide concentrations over the North Pacific Ocean, Tellus B, 44, 161–172, https://doi.org/10.3402/tellusb.v44i3.15438, 1992.

Nakazawa, T., Machida, T., Sugawara, S., Murayama, S., Morimoto, S., Hashida, G., Honda, H., and Itoh, T.: Measurements of the stratospheric carbon dioxide concentration over Japan using a balloon-borne cryogenic sampler, Geophys. Res. Lett., 22, 1229–1232, https://doi.org/10.1029/95GL01188, 1995.

Pales, J. C. and Keeling, C. D.: The concentration of atmospheric carbon dioxide in Hawaii, J. Geophys. Res., 70, 6053–6076, https://doi.org/10.1029/JZ070i024p06053, 1965.

Stephens, B. B., Gurney, K. R., Tans, P. P., Sweeney, C., Peters, W., Bruhwiler, L., Ciais, P., Ramonet, M., Bousquet, P., Nakazawa, T., Aoki, S., Machida, T., Inoue, G., Vinnichenko, N., Lloyd, J., Jordan, A., Heimann, M., Shibistova, O., Langenfelds, R. L., Steele, L. P., Francey, R. J., and Denning, A. S.: Weak northern and strong tropical land carbon uptake from vertical profiles of atmospheric CO_2, Science, 316, 1732–1735, https://doi.org/10.1126/science.1137004, 2007.

Sweeney, C., Karion, A., Wolter, S., Newberger, T., Guenther, D., Higgs, J. A., Andrews, A. E., Lang, P. M., Neff, D. Dlugokencky, E., Miller, J. B., Montzka, S. A., Miller, B. R., Masarie, K. A., Biraud, S. C., Novelli, P. C., Crotwell, M., Crotwell, A. M., Thoning, K., and Tans, P. P.: Seasonal climatology of CO_2 across North America from aircraft measurements in the NOAA/ESRL Global Greenhouse Gas Reference Network, J. Geophys. Res., 120, 5155–5190, https://doi.org/10.1002/2014JD022591, 2015.

Tanaka, M., Nakazawa, T., and Aoki, S.: High quality measurements of the concentration of atmospheric carbon dioxide, J. Meteorol. Soc. Jpn., 61, 678–685, https://doi.org/10.2151/jmsj1965.61.4_678, 1983.

Tanaka, M., Nakazawa, T., and Aoki, S.: Time and space variations of tropospheric carbon dioxide over Japan, Tellus B, 39, 3–12, https://doi.org/10.3402/tellusb.v39i1-2.15318, 1987.

Tanaka, T., Miyamoto, Y., Morino, I., Machida, T., Nagahama, T., Sawa, Y., Matsueda, H., Wunch, D., Kawakami, S., and Uchino, O.: Aircraft measurements of carbon dioxide and methane for the calibration of ground-based high-resolution Fourier Transform Spectrometers and a comparison to GOSAT data measured over Tsukuba and Moshiri, Atmos. Meas. Tech., 5, 2003–2012, https://doi.org/10.5194/amt-5-2003-2012, 2012.

Tans, P. P., Conway, T., and Nakazawa, T.: Latitudinal distribution of the sources and sinks of atmospheric carbon dioxide derived from surface observations and an Atmospheric Transport Model, J. Geophys. Res., 94, 5151–5172, https://doi.org/10.1029/JD094iD04p05151, 1989.

Watai, T., Machida, T., Ishizaki, N., and Inoue, G.: A lightweight observation system for atmospheric carbon dioxide concentration using a small unmanned aerial vehicle, J. Atmos. Ocean. Tech., 23, 700–710, https://doi.org/10.1175/JTECH1866.1, 2006.

Winderlich, J., Chen, H., Gerbig, C., Seifert, T., Kolle, O., Lavrič, J. V., Kaiser, C., Höfer, A., and Heimann, M.: Continuous low-maintenance $CO_2/CH_4/H_2O$ measurements at the Zotino Tall Tower Observatory (ZOTTO) in Central Siberia, Atmos. Meas. Tech., 3, 1113–1128, https://doi.org/10.5194/amt-3-1113-2010, 2010.

WMO: The state of greenhouse gases in the atmosphere using global observations through 2015, WMO Greenhouse Gas Bull., 12, 1–8, 2016.

Wofsy, S. C., the HIPPO science team, and cooperating modellers and satellite teams: HIAPER Pole-to-Pole Observations (HIPPO): fine-grained, global-scale measurements of climatically important atmospheric gases and aerosols, Philos. T. R. Soc. A, 369, 2073–2086, https://doi.org/10.1098/rsta.2010.0313, 2011.

Wunch, D., Toon, G. C., Blavier, J. L., Washenfelder, R. A., Notholt, J., Connor, B. J., Griffith, D. W. T., Sherlock, V., and Wennberg, P. O.: The Total Carbon Column Observing Network, Philos. T. R. Soc. A, 369, 2087–2112, https://doi.org/10.1098/rsta.2010.0240, 2011.

Yokota, T., Yoshida, Y., Eguchi, N., Ota, Y., Tanaka, T., Watanabe, H., and Maksyutov, S.: Global concentrations of CO_2 and CH_4 retrieved from GOSAT: First preliminary results, Sci. Online Lett. Atmos., 5, 160–163, https://doi.org/10.2151/sola.2009-041, 2009.

Yoshida, Y., Ota, Y., Eguchi, N., Kikuchi, N., Nobuta, K., Tran, H., Morino, I., and Yokota, T.: Retrieval algorithm for CO_2 and CH_4 column abundances from short-wavelength infrared spectral observations by the Greenhouse gases observing satellite, Atmos. Meas. Tech., 4, 717–734, https://doi.org/10.5194/amt-4-717-2011, 2011.